NASA

Technical Memorandum **83857**

On the Theory of Gamma Ray Amplification Through Stimulated Annihilation Radiation (GRASAR)

R. Ramaty
J. M. McKinley
F. C. Jones

NOVEMBER 1981

National Aeronautics and
Space Administration

Goddard Space Flight Center
Greenbelt, Maryland 20771

ON THE THEORY OF GAMMA RAY AMPLIFICATION THROUGH STIMULATED ANNIHILATION RADIATION (GRASAR)

R. Ramaty

J. M. McKinley*

F. C. Jones

Laboratory for High Energy Astrophysics,

NASA/Goddard Space Flight Center,

Greenbelt, Maryland 20771

Accepted for publication in the Astrophysical Journal

*Also at Oakland University, Rochester, Michigan 48063 and the University of Maryland, College Park, Maryland 20742

Abstract

The theory of photon emission, absorption and scattering in a relativistic plasma of positrons, electrons and photons is studied. Expressions for the emissivities and absorption coefficients of pair annihilation, pair production and Compton scattering are given and evaluated numerically. The conditions for negative absorption are investigated. In a system of photons and e^+-e^- pairs, an emission line at ~ 0.43 MeV can be produced by grasar action provided that the pair chemical potential exceeds ~ 1 MeV. At a temperature of ~ 10^9K this requires a pair density $\gtrsim 10^{30}$cm^{-3}, a value much larger than the thermodynamic equilibrium pair density at this temperature. This emission line could account without a gravitational redshift for the observed lines at this energy from gamma ray bursts.

I. Introduction

The emission and absorption of photons in cosmic sources are governed by many processes. At temperatures of the order 10^9 to 10^{10}K, typical of gamma ray burst sources, two of the most important ones are pair production and annihilation ($e^+ + e^- \rightleftarrows \gamma + \gamma$) and Compton and inverse Compton scattering ($e + \gamma \rightleftarrows e' + \gamma'$). Arguments based on the observed photon intensities of gamma ray bursts and the likely distances and sizes of their sources, lead to the conclusion that the source regions of at least some of the bursts are optically thick (Cavallo and Rees 1978, Schmidt 1978).

Photon absorption in $\gamma\gamma$ pair production has been discussed in the literature (Gould and Schreder 1967), but no calculation has included the effects of the stimulation of the annihilation or the suppression of pair production due to large photon or particle occupation numbers. When these stimulation and suppression effects are taken into account, the possibility exists for negative absorption (Varma 1977). The condition for this is a population inversion, which in the present context is a pair density that exceeds the thermodynamic equilibrium density.

A recent review of gamma ray burst observations has been given by Cline (1981). Of particular interest for the present paper is the existence of an emission line seen from several gamma ray bursts in the energy range from 0.40 to 0.46 MeV (Mazets et al. 1979, Teegarden and Cline 1980, Mazets et al. 1981). These lines are probably due to e^+-e^- annihilation radiation. If so, e^+-e^- pairs should be present in large numbers in the burst sources, and the sources should be sufficiently hot to produce the pairs, but the source regions should not be in thermodynamical equilibrium because no lines can then be seen. We aim the calculations of the present paper to astrophysical sites where such conditions might exist.

We provide the basic analytic treatment in Section II, we give numerical results in Section III, we discuss some astrophysical applications in Section IV, and give our conclusions in Section V.

II. Emissivities and Absorption Coefficients in a Relativistic Plasma

We consider systems characterized by temperatures of the order of the electron rest mass energy in which photon-photon collisions can produce much larger pair densities than the ambient electron densities of the astrophysical sites of interest. We therefore consider only cases in which the electrons and positrons have equal densities. As convenient analytical expressions, which allow both equilibrium and non-equilibrium situations, we use Bose-Einstein distributions for the photons and Fermi-Dirac distributions for the pairs (see Landau and Lifshitz 1958). The reference frame in which these distributions are isotropic is designated as the plasma frame.

We assume equal temperatures for the positrons and electrons, $T_+ = T_- = T_\pm$, but allow the photon temperature, T_γ, to differ from $T_\pm$. Since the e^+ and e^- densities are equal, $n_+ = n_- = n_\pm$, these particles must also have equal chemical potentials, $\mu_+ = \mu_- = \mu_\pm$. The photon chemical potential, μ_γ, is zero for a blackbody distribution. We allow non-blackbody photon distributions, but only zero or negative values may be assigned to μ_γ. The pair chemical potential can be positive, zero or negative. If $\mu_\pm = 0$ the pairs are in thermodynamic equilibrium with blackbody photons.

In terms of these temperatures and chemical potentials, the photon and pair densities can be written as (e.g. Landau and Lifshitz 1958)

$$n = (4\pi^3\hbar^3)^{-1}\int d^3p\, n \quad , \tag{1}$$

where $\vec{p}$ is the photon or particle momentum and n is the occupation number. These are given by

$$n_\gamma = \{\exp[(E_\gamma - \mu_\gamma)/kT_\gamma] - 1\}^{-1} \qquad (2)$$

for the photons, and by

$$n_\pm = \{\exp[(E_\pm - \mu_\pm)/kT_\pm] + 1\}^{-1} \qquad (3)$$

for the particles, where E_γ is the photon energy and $E_\pm$ is the particle total energy (kinetic plus rest mass). Equation (1) counts both polarization states for the photons and both spin states for the particles.

The blackbody ($\mu_\gamma = 0$) photon density is shown by the line γ in Figure 1. This quantity has the simple analytic form $n_\gamma = 2\zeta(3)\pi^{-2}(kT/c\hbar)^3$, where $\zeta(3) = 1.2021....$ The other curves in this figure show pair densities for various chemical potentials $\mu_\pm$. Pair densities corresponding to positive or negative $\mu_\pm$ yield higher or lower pair annihilation rates, respectively, than the pair production rate of blackbody radiation. The Fermi-Dirac distributions (equation 3) tend to Maxwell-Boltzmann distributions in the limit of large $-\mu_\pm$.

We proceed to define the photon emissivity and absorption coefficient for pair production and annihilation. In particular, we are interested in obtaining a correct expression for stimulated annihilation which has not been taken into account in previous treatments of absorption in photon-photon pair production. Stimulated emission has, of course, been taken into account for other processes (e.g. Bekefi 1966). But we cannot use the standard expressions for emissitivies and absorption coefficients because pair

production and annihilation do not fit the usual pattern in which photons are emitted or absorbed singly and the matter has the same form before and after events. We therefore proceed as follows:

For two-photon annihilation and pair production, $e^+ + e^- \rightleftarrows \gamma_1 + \gamma_2$, the transition rate in vacuum in either direction between the photon states in $d^3p_1 d^3p_2$ and the pair states in $d^3p_+ d^3p_-$ can be written as

$$w = (4\pi^3\hbar^3)^{-2}\, d^3p_1 d^3p_2 d^3p_+ d^3p_-\, \delta^4(p_1+p_2-p_+-p_-)X. \qquad (4)$$

Here $\vec{p}_1$ and $\vec{p}_2$ are photon momenta, $\vec{p}_+$ and $\vec{p}_-$ are momenta of the pair, p_1, p_2, p_+ and p_- are the corresponding 4-momenta, and X is proportional to the squared matrix element of the interaction, summed and averaged over spins and polarization.

To obtain the total annihilation and pair production rates we must multiply equation (4) by an appropriate combination of the occupation numbers. This can be obtained from energy conservation ($E_1+E_2 = E_+ + E_-$) and the equilibrium condition ($\mu_\pm = \mu_\gamma$ and $T_\pm = T_\gamma$) , where E_1 and E_2 are the energies of the two photons. Equations (2) and (3) then yield

$$n_1 n_2 (1-n_+)(1-n_-) = n_+ n_- (1+n_1)(1+n_2) \quad . \qquad (5)$$

Multiplying both sides of this equation by the transition rate (equation 4) and integrating over all four momenta, we obtain

$$\frac{1}{2}\int \frac{n_+ d^3p_+}{4\pi^3\hbar^3}\int \frac{n_- d^3p_-}{4\pi^3\hbar^3}\int d\Omega_1\ (1+n_1)(1+n_2)\left[Ic\frac{d\sigma}{d\Omega}\right]_{ann} =$$

$$= \frac{1}{2}\int \frac{n_1 d^3p_1}{4\pi^3\hbar^3}\int \frac{n_2 d^3p_2}{4\pi^3\hbar^3}\int d\Omega_+ (1-n_+)(1-n_-)\left[Ic\,\frac{d\sigma}{d\Omega}\right]_{pp}. \qquad (6)$$

The left-hand side of equation (6) is the total pair annihilation rate, while the right-hand side is the total pair production rate. The invariant product of the flux factor I and differential cross section $d\sigma/d\Omega$ (Jauch and Rorlich 1955) is obtained from X by integration over all final state variables except the angles of one particle:

$$[Ic\,\frac{d\sigma}{d\Omega}]_{ann} = \int p_1^{\,2} dp_1 \int p_2^{\,2} dp_2 \int d\Omega_2 \delta^4(p_1+p_2-p_+-p_-)X \qquad (7)$$

$$[Ic\,\frac{d\sigma}{d\Omega}]_{pp} = \int p_+^{\,2} dp_+ \int p_-^{\,2} dp_- \int d\Omega_- \delta^4(p_1+p_2-p_+-p_-)X. \qquad (8)$$

The factor $1/2$ in equation (6) is introduced so that each distinct pair of photons in either initial or final state is included just once. Note that the annihilation is stimulated by the presence of the bath of photons, while pair production is suppressed by the presence of the bath of pairs. However, if $\mu_\pm = \mu_\gamma << 0$, the pair and photon distributions are reduced to Maxwell-Boltzmann distributions and this removes all the stimulation and degeneracy effects.

To define a photon emissivity and absorption coefficient it is necessary to investigate the balance of reactions involving photons in an increment d^3p_1. We proceed as in the derivation of equation (6), except that the integration extends only over d^3p_2, d^3p_+, and d^3p_-. In this case, however, it is no longer possible to express the left side in terms of the annihilation cross section, because the necessary integration of equation (7) has not been performed. But we can interchange the order of integration and use equation (8) instead. The required balance is then given by

$$\frac{(1+\eta_1)d^3p_1}{4\pi^3\hbar^3}\int \frac{d^3p_2}{4\pi^3\hbar^3}\int d\Omega_+\eta_+\eta_-(1+\eta_2)\left[Ic\,\frac{d\sigma}{d\Omega}\right]_{pp} =$$

$$= \frac{\eta_1 d^3p_1}{4\pi^3\hbar^3}\int \frac{d^3p_2}{4\pi^3\hbar^3}\int d\Omega_+\eta_2(1-\eta_+)(1-\eta_-)\left[Ic\,\frac{d\sigma}{d\Omega}\right]_{pp}. \qquad (9)$$

Collecting terms in η_1, we obtain

$$dE_1 d\Omega_1 j_{\gamma\gamma}(E_1) = \frac{c\eta_1 E_1^2 dE_1 d\Omega_1}{4\pi^3(\hbar c)^3}\, K_{\gamma\gamma}(E_1), \qquad (10)$$

where the rate of spontaneous emission, $j_{\gamma\gamma}(E_1)$, and coefficient of linear absorption, $K_{\gamma\gamma}(E_1)$, are given by

$$j_{\gamma\gamma}(E_1) = \frac{cE_1^2}{4\pi(\hbar c)^3}\int\frac{d^3p_2}{4\pi^3\hbar^3}\int d\Omega_+\eta_+\eta_-(1+\eta_2)\left[I\,\frac{d\sigma}{d\Omega}\right]_{pp} \qquad (11)$$

and

$$K_{\gamma\gamma}(E_1) = \int\frac{d^3p_2}{4\pi^3\hbar^3}\int d\Omega_+\left[\eta_2(1-\eta_+)(1-\eta_-) - \eta_+\eta_-(1+\eta_2)\right]\left[I\frac{d\sigma}{d\Omega}\right]_{pp}. \qquad (12)$$

In equation (11) the annihilation emissivity is expressed in terms of the pair production cross section unlike the approach where this is done in terms of the annihilation cross section (e.g. Ramaty and Mészáros 1981). In the expression for the absorption coefficient (equation 12), the first term in the brackets is due to absorption by the photon bath while the second term is the contribution of induced annihilation. When the equilibrium condition (5) is satisfied and $\mu_\gamma = 0$, equations (11) and (12) yield Kirchhoff's law,

$$j_{\gamma\gamma}/K_{\gamma\gamma} = \frac{c}{4\pi^3(\hbar c)^3}\,\frac{E_1^2}{\exp(E_1/kT)-1} \equiv I_{BB}(E_1), \qquad (13)$$

where I_{BB} is the blackbody intensity.

Equations (11) and (12) are valid also for nonequilibrium situations provided proper nonequilibrium occupation numbers are used. In terms of equations (2) and (3), the most general nonequilibrium distributions are obtained if $T_\gamma \neq T_\pm$ and $\mu_\gamma \neq \mu_\pm$. With such distributions, the total annihilation and pair production rates are not equal and, moreover, $K_{\gamma\gamma}$ can become negative. While for $T_\pm = T_\gamma$ and $\mu_\pm = \mu_\gamma$, $K_{\gamma\gamma}$ is always positive, for nonequilibrium conditions the contribution of stimulated annihilation can exceed that of absorption provided an appropriate population inversion takes place. By substituting equations (2) and (3) into equation (12) we find that for $T_\pm = T_\gamma$ such an inversion occurs if $2\mu_\pm > \mu_\gamma$. In this case $K_{\gamma\gamma}$ is negative for $E_1 < 2\mu_\pm - \mu_\gamma$.

For the system to exhibit grasar action, however, it is necessary that the total absorption coefficient be negative. For the system of photons and pairs that we consider here, the only important process other than pair production and annihilation is Compton scattering. We ignore the weaker processes of bremsstrahlung and double Compton scattering. We note, however, that synchrotron radiation could potentially be very important, but because we are free to choose an arbitrarily low magnetic field intensity, we ignore synchrotron absorption in the present discussion.

For Compton and inverse Compton scatterings ($\gamma_1 + e \rightleftarrows \gamma_2 + e'$) we proceed in essentially the same way as for pair production and annihilation. Using $\vec{p}_1$ and $\vec{p}_2$ for photon momenta and $\vec{p}$ and $\vec{p}'$ for electron and positron momenta, we find the equation for the overall balance between inverse Compton scattering and direct Compton scattering to be

$$2\int \frac{n_\pm' d^3p'}{4\pi^3\hbar^3} \int \frac{n_2 d^3p_2}{4\pi^3\hbar^3} \int d\Omega_1 (1+n_1)(1-n_\pm)\left[Ic \frac{d\sigma}{d\Omega}\right]_{C'} =$$

$$= 2\int \frac{\eta_t d^3p}{4\pi^3\hbar^3}\int \frac{\eta_1 d^3p_1}{4\pi^3\hbar^3}\int d\Omega_2(1+\eta_2)(1-\eta_t')[Ic\ \frac{d\sigma}{d\Omega}]_C \quad , \tag{14}$$

where the factor of 2 takes into account the contributions of both electrons and positrons. Here again the invariant product of flux factor and differential cross section is given by integrating the appropriate squared matrix element over all final state variables except the photon angles. For the direct scattering we have

$$[Ic\ \frac{d\sigma}{d\Omega}]_C = \int p_2^{\,2} dp_2 \int p'^{\,2} dp' \int d\Omega' \delta^4(p_1+p-p_2-p')X_C. \tag{15}$$

For the inverse scattering, designated by subscript C', the same form applies with the substitutions $\vec{p}_2 \rightarrow \vec{p}_1$ and $\vec{p}' \rightarrow \vec{p}$. Equation (14) is valid for any choice of $\mu_\pm$ and μ_γ as long as $T_\pm = T_\gamma$.

To obtain expressions for the emissivity and absorption coefficient, we again choose an increment d^3p_1 and integrate over the other three momenta. As for pair production and annihilation, we must interchange the order of integrations on one side in order to introduce a cross section. After the appropriate manipulations we obtain the Compton emissivity and absorption coefficient in the presence of the bath of photons and pairs

$$j_C(E_1) = \frac{cE_1^{\,2}}{4\pi^3(\hbar c)^3} 2\int \frac{d^3p}{4\pi^3\hbar^3}\int d\Omega_2 \eta_2 \eta_t'(1-\eta_t)[I\frac{d\sigma}{d\Omega}]_C \quad , \tag{16}$$

$$K_C(E_1) = 2\int\frac{d^3p}{4\pi^3\eta^3}\int d\Omega_2 [n_\pm(1+n_2)(1-n'_\pm)-n_2n'_\pm(1-n_\pm)][I\frac{d\sigma}{d\Omega}]_C \ . \qquad (17)$$

The Compton emissivity, equation (16), represents the scatterings of photons 2 into the element $dE_1 d\Omega_1$. For the absorption coefficient, equation (17), the first term in the brackets is due to scattering of photons out of $dE_1 d\Omega_1$, while the second term represents the stimulated scatterings of photons 2 into $dE_1 d\Omega_1$. $K_C(E_1)$ can become negative and a necessary condition for this is $T_\gamma > T_\pm$. In our subsequent analysis, however, we shall only consider systems with $T_\gamma = T_\pm$ for which K_C is always positive. In such cases equations (16) and (17) satisfy a modified Kirchhoff's law

$$j_C(E_1)/K_C(E_1) = \frac{cE_1^2}{4\pi^3(\hbar c)^3}[\exp[(E_1-\mu_\gamma)/kT_\gamma]-1)^{-1}. \qquad (18)$$

For the numerical evaluations shown below we have used the expressions of Jauch and Rohrlich (1955) for the flux factors and differential cross sections. We must also express all quantities in terms of independent variables of integration. For pair production from photons of energies E_1 and E_2, the flux factor is given by

$$I_{pp} = 1- \cos\theta_{12}, \qquad (19)$$

where θ_{12} is the angle between the two photons in the plasma frame. In the center-of-momentum frame (CM frame), the positron (or electron) has Lorentz factor γ given by

$$(\gamma mc^2)^2 = \tfrac{1}{2} E_1 E_2 (1-\cos\theta_{12}) \quad . \tag{20}$$

The Lorentz factor γ_{CM} for the tranformation between plasma frame and CM frame is

$$\gamma_{CM} = (E_1+E_2)/(2\gamma mc^2) \quad . \tag{21}$$

The velocity associated with γ_{CM} is β_{CM}. In the CM frame the direction of the positron is given by colatitude θ from the direction of photon 1 and azimuth ϕ from the plane of β_{CM} and photon 1. The electron direction is diametrically opposite. The differential cross section is

$$\left[\frac{d\sigma}{d\Omega}\right]_{pp} = \frac{r_o^2 \beta}{4\gamma^2} \frac{1-\beta^2\cos^4\theta+2\gamma^{-2}\beta^2\sin^2\theta}{(1-\beta^2\cos^2\theta)^2}, \tag{22}$$

where r_o is the classical electron radius (2.818×10^{-13}cm)and $\beta = (1-\gamma^{-2})^{1/2}$. The angle θ_1 between photon 1 and β_{CM} is given by

$$\cos\theta_1 = \beta_{CM}^{-1}[E_1(\gamma_{CM}\gamma mc^2)^{-1}-1], \tag{23}$$

and the angle θ_+ between the positron and β_{CM} is

$$\cos\theta_+ = \cos\theta_1\cos\theta+\sin\theta_1\sin\theta\cos\phi. \tag{24}$$

Finally the energies of the pair in the plasma frame are given by

$$E_\pm = \gamma_{CM}\gamma mc^2(1\pm\beta_{CM}\beta\cos\theta_+), \tag{25}$$

and the occupation numbers are given by equations (2) and (3). Thus everything needed to evaluate equations (11) and (12) has been found from E_1, E_2, θ_{12}, θ, and ϕ . A Monte-Carlo technique was used to evaluate the four-dimensional integrals over E_2, θ_{12}, θ, and ϕ .

For Compton scattering all quantities can be evaluated directly in the plasma frame, thanks to expressions given by Jauch and Rohrlich (1955). For an initial photon of energy E_1 and an initial electron or positron of energy

$$E_{\pm} = \gamma_{\pm} mc^2 = mc^2(1-\beta_{\pm}^2)^{-1/2}, \tag{26}$$

the flux factor is given by

$$I_C = 1-\beta_{\pm}\cos\alpha_1, \tag{27}$$

where α_1 is the angle between electron and photon. The direction of the scattered photon (photon 2) is given by colatitude θ from the direction of photon 1 and azimuth ϕ from the plane of photon 1 and the initial electron. The angle α_2 between photon 2 and the initial electron is given by

$$\cos\alpha_2 = \cos\alpha_1\cos\theta + \sin\alpha_1\sin\theta\cos\phi. \tag{28}$$

The energy E_2 of photon 2 is given by

$$\frac{E_2}{E_1} = \frac{1-\beta_{\pm}\cos\alpha_1}{1+(E_1/E_{\pm})(1-\cos\theta)-\beta_{\pm}\cos\alpha_2} \tag{29}$$

The differential cross section is

$$\left[\frac{d\sigma}{d\Omega}\right]_C = \frac{1}{2}\left[\frac{r_o E_2}{\gamma_\pm E_1(1-\beta_\pm\cos\alpha_1)}\right]^2\left[\frac{k_1}{k_2}+\frac{k_2}{k_1}+2\left(\frac{mc^2}{k_1}-\frac{mc^2}{k_2}\right)+\left(\frac{mc^2}{k_1}-\frac{mc^2}{k_2}\right)^2\right], \quad (30)$$

where the invariants k_1 and k_2 are

$$k_1 = E_1\gamma_\pm(1-\beta_\pm\cos\alpha_1) \quad (31)$$

$$k_2 = E_2\gamma_\pm(1-\beta_\pm\cos\alpha_2). \quad (32)$$

The energy of the final electron is

$$E'_\pm = E_\pm + E_1 - E_2 \quad , \quad (33)$$

and the occupation numbers can be found from equations (2) and (3). Again everything needed to evaluate equations (16) and (17) has been found in terms of E_1, $E_\pm$, α_1, θ, and ϕ. A Monte-Carlo technique was used to evaluate the four-dimensional integrals over $E_\pm$, α_1, θ, and ϕ.

III. Numerical Results

We have evaluated equations (11), (12), (16) and (17) for various choices of $T_\pm$, T_γ, $\mu_\pm$ and μ_γ. As already indicated, we limit our discussion here to cases with equal pair and photon temperatures, $T_\pm = T_\gamma \equiv T$. We allow, however, arbitrary values for $\mu_\pm$ and μ_γ.

We consider first the case of thermodynamic equilibrium, $\mu_\pm = \mu_\gamma = 0$. The emissivities and absorption coefficients for this case and $T = 3\times10^9$K are shown in Figure 2, where $j_t = j_{\gamma\gamma} + j_C$ and $K_t = K_{\gamma\gamma} + K_C$. As can be seen, the absorption coefficients are positive at all photon energies and Kirchhoff's law is satisfied by all processes.

We next consider a case of equilibrium between pair annihilation and pair production by non blackbody photons. Numerical results for $\mu_\pm = \mu_\gamma = -2$ MeV

and $T = 3 \times 10^9 K$ are shown in Figure 3. Because for these parameters both the particle and photon occupation numbers are very small ($<10^{-3}$), the results of Figure 3 closely approximate emissivities and absorption coefficients appropriate for Maxwell-Boltzmann distributions. Indeed, the emissivity $j_{\gamma\gamma}$ shown in Figure 3 is essentially identical with the annihilation emissivity calculated by Ramaty and Mészáros (1981) using a Maxwell-Boltzmann distribution and the pair annihilation cross section. As discussed by these authors, as well as Zdziarski (1981) and Aharonian, Atoyan and Sunyaev (1980), the peak of the annihilation emissivity occurs at a higher energy than $mc^2 = 0.511$ MeV, because the annihilation photons must carry away the kinetic energies of the pairs in addition to their rest mass energy. This effect is very obvious in both Figures 2 and 3.

From the emissivity $j_{\gamma\gamma}$ of Figure 3 we can evaluate the full width at half maximum (FWHM) of an optically thin annihilation feature produced in a Maxwellian plasma of $T_\pm = 3 \times 10^9 K$. We find that for this temperature the FWHM ($\sim$ 850 keV) is in excellent agreement with the calculations of Ramaty and Mészáros (1981) who deduced the dependence of FWHM on $T_\pm$ for such plasmas. The absorption coefficients of Figure 3 are positive at all energies. While Kirchhoff's law is not satisfied (because $\mu_\gamma \neq 0$), the j's and K's of Figure 3 do satisfy the modified Kirchhoff's law (equation 18) for all processes.

We turn now to the study of cases with inverted populations. For $T_\pm = T_\gamma$ the inversion condition is $\mu_\pm > \mu_\gamma/2$. Since $\mu_\gamma < 0$, the inversion threshold is at a value of $\mu_\pm$ that is higher than or equal to the value at which pair production and annihilation are in equilibrium, $\mu_\pm = \mu_\gamma$. The two values are equal for blackbody photons, $\mu_\gamma = 0$. When an inversion occurs, $K_{\gamma\gamma}$ is negative for $E_\gamma < 2\mu_\pm - \mu_\gamma$, but since $T_\pm = T_\gamma$, K_C is positive for all E_γ. Grasar action can occur only if $K_t = K_{\gamma\gamma} + K_C < 0$. Since K_C is proportional to

$n_\pm$ while the portion of $K_{\gamma\gamma}$ due to stimulated annihilation varies as $n_\pm^2$, a sufficiently large density is needed for $-K_{\gamma\gamma}$ to exceed K_C. This implies a threshold for $\mu_\pm$ which is higher than the threshold required for just $K_{\gamma\gamma}$ to be negative.

To investigate this threshold we have evaluated $K_t = K_{\gamma\gamma} + K_C$ as a function of $\mu_\pm$ for given temperatures and μ_γ. We have carried out calculations in the temperature range $0 < T < 5\times10^9$K, where the lower limit corresponds to fully degenerate electrons and positrons. We find that the threshold for grasar action is close to $\mu_\pm = 1$ MeV and does not depend strongly on μ_γ and T. As can be seen from Figure 1, this corresponds to a pair density threshold of a few times 10^{30}cm^{-3}.

We show numerical results in Figure 4 for $T = 3\times10^9$K, $\mu_\gamma = 0$ and $\mu_\pm = 1.1$ MeV. As can be seen, $K_{\gamma\gamma}$ is negative for $E_\gamma < 2\mu_\pm = 2.2$ MeV and positive at higher energies. K_C is positive at all energies and Kirchhoff's law ($j_C/K_C = I_{BB}$) is satisfied for Compton scattering since $\mu_\gamma = 0$. In the energy range from about 0.25 MeV to 0.7 MeV, $-K_{\gamma\gamma}$ exceeds K_C and hence K_t is negative. If the source is optically thick and K_t is negative over a sufficiently large spatial region, then the radiation intensity has a sharp peak at a photon energy at which $-K_t$ is maximal. The value of this energy, ~ 0.43 MeV from the numerical calculations, is determined primarily from the energy at which $-K_{\gamma\gamma}$ is maximum, shifted somewhat according to the slope of K_C at that energy. From Equation (12) we can also express $K_{\gamma\gamma}$ in the form

$$K_{\gamma\gamma}(E_\gamma) = -\frac{4\pi^3(\hbar c)^3}{cE_\gamma^2} j_{\gamma\gamma}(E_\gamma) + \int\frac{d^3p_2}{4\pi^3\hbar^3}\int d\Omega_+ n_2(1-n_+)(1-n_-)\left[I\frac{d\sigma}{d\Omega}\right]_{pp} . \quad (34)$$

Above the grasar action threshold, the first term, due to stimulated emission,

is much larger in magnitude than the second term which is due to absorption. As discussed above, $j_{\gamma\gamma}(E_\gamma)$ is broadly peaked at an energy greater than mc^2, reflecting the kinetic energy of the annihilating pairs. The division by E_γ^2 (from the factor of density of states) shifts the peak to an energy somewhat less than mc^2.

The most extreme case of population inversion arises when $T_\gamma = T_\pm = 0$. The system then includes no thermal photons at all. The particle states are fully occupied or degenerate ($n_\pm = 1$) up to the Fermi momentum p_F, and are empty ($n_\pm = 0$) above p_F. The Fermi momentum is related to the chemical potential by

$$cp_F = (\mu_\pm^2 - m^2c^4)^{1/2}, \tag{35}$$

and to the pair density by

$$n_\pm = (3\pi^2\hbar^3)^{-1} p_F^3. \tag{36}$$

At $T_\gamma = 0$ there is no absorption term in $K_{\gamma\gamma}$ because there are no photons in the bath. Therefore $K_{\gamma\gamma}$ can only be zero or negative and is proportional to $j_{\gamma\gamma}$:

$$K_{\gamma\gamma}(E_\gamma) = -\frac{4\pi^3(\hbar c)^3}{cE_\gamma^2} j_{\gamma\gamma}(E_\gamma). \tag{37}$$

Both $j_{\gamma\gamma}$ and $K_{\gamma\gamma}$ are non-zero only between the kinematic limits

$$\mu_\pm - cp_F < E_\gamma < \mu_\pm + cp_F. \tag{39}$$

These limits correspond to the annihilation of a pair with equal momenta of

magnitude p_F into one photon with momentum parallel to the pair momenta (upper kinematic limit) and another photon with momentum antiparallel to the pair momenta (lower kinematic limit).

Similarly, $j_C = 0$ and there is no stimulated emission term in K_C because there are no photons present to be scattered to contribute these effects. Only the absorption term in K_C is present, so that K_C is necessarily positive. For small E_γ, only those particles with momentum near P_F can contribute to K_C, because the particle can only be scattered into a previously unoccupied state.

Numerical results are shown in Figure 5 for $T = 0$, $\mu_\gamma = 0$ and $\mu_\pm = 0.85$ MeV. Here the broadening of $j_{\gamma\gamma}$ is caused by the motion of the degenerate particles even though their temperature $T_\pm = 0$. We shall refer to this effect as degeneracy broadening. By evaluating $j_{\gamma\gamma}$ for other values of $\mu_\pm$ as well, we find that the FWHM for degeneracy broadening is proportional to the Fermi momentum p_F, and hence proportional to $n_\pm^{1/3}$ for both non-relativistic ($p_F \ll mc$) and relativistic ($p_F > mc$) degenerate distributions. It is given by

$$\text{FWHM} = (4.3 \times 10^{-8}\ \text{keV})\ n_\pm^{1/3} \tag{40}$$

when $n_\pm$ is expressed in cm^{-3}.

In Figure 5 the kinematical limits on $j_{\gamma\gamma}$ and $K_{\gamma\gamma}$ are quite evident, as is the suppression of K_C by degeneracy at low photon energies. The peak of $j_{\gamma\gamma}$ is at about 0.75 MeV, but because of the E_γ^{-2} factor in equation (34), the peak of $-K_{\gamma\gamma}$ is shifted to about 0.50 MeV. Because of the steep positive slope of K_C, the peak of $-K_t$ in Figure 5 is further shifted to about 0.42 MeV.

From the numerical calculations for other values of T and $\mu_\pm$

($0<T<5\times10^9$K, $0.8<\mu_\pm<1.2$ MeV) we find that the peak of $-K_t$ is invariably in the energy range from about 0.40 to 0.47 MeV. When $\mu_\pm$ is close to the threshold for grasar action, the peak energy of $-K_{\gamma\gamma}$ decreases with increasing temperature, but the varying slope of K_C resulting from the degeneracy tends to cancel this effect. Thus, there is not much variation of the peak energy of $-K_t$ with either T or $\mu_\pm$. For the parameters considered, we have found no case when the peak energy of $-K_t$ equaled or exceeded 0.5 MeV.

III. Astrophysical Applications

Gamma ray burst sources are likely astrophysical sites where the results of the present paper could be applied. The large photon densities expected (Cavallo and Rees 1978, Schmidt 1978) in these sources should lead to high pair production and Compton opacities. The observation (Mazets et al. 1979, Teegarden and Cline 1980, Mazets et al. 1981) of an emission line in the energy range 0.4 to 0.46 MeV, believed to be due to e^+-e^- annihilation radiation, is evidence that e^+-e^- pairs do indeed play an important role in the physics of gamma ray bursts. But it is not immediately obvious how a relatively narrow emission line is produced in a hot and optically thick source region.

Ramaty et al. (1980) and Ramaty, Lingenfelter and Bussard (1981) have studied this problem and discussed an optically thin model for the transient of March 5, 1979 (Barat et al. 1979, Cline et al. 1980, Evans et al. 1980) from which an emission line was observed (Mazets et al., 1979) at ~ 0.43 MeV. In this model, the ~ 0.43 MeV line is formed at an energy $\gtrsim$ 0.511 MeV in the last optical depth of the source region by the annihilation of e^+-e^- pairs that have been cooled by synchrotron radiation prior to their annihilation. The shift from above mc^2 to the observed energy is due to the gravitational redshift of a neutron star. The observed upper limit on the

width (FWHM $\lesssim$ 0.2 MeV, Mazets et al. 1979, 1981) implies a temperature less than 3×10^8K (Ramaty and Mészáros 1981). The upper limit on the width also implies an upper limit on the density because of degeneracy broadening. Using equation (40) we obtain $n_\pm \lesssim 7\times10^{28}\text{cm}^{-3}$ for the e^+-e^- annihilation region if the line is produced by annihilation in the last optical depth.

The density $n_\pm$ can also be directly calculated (Ramaty et al. 1981) from the observed line fluence ($\phi \approx 10$ photons cm^{-2}, Mazets et al. 1979). Let $R/(n_\pm)^2 \approx 7.5\times10^{-15}\text{cm}^3\text{sec}^{-1}$ be the annihilation rate coefficient at 3×10^8K (Ramaty and Mészáros 1981), A the area of the emitting region, Δt the time interval in which the observed fluence is produced and d = 55kpc the distance to the source. Then if the line is formed in a layer of unit optical depth to Compton scattering,

$$\phi \approx 2R\, K_C^{-1}\, A\Delta t\, (4\pi d^2)^{-1} \tag{41}$$

Since R varies as $n_\pm^2$ and K_C^{-1} as $n_\pm^{-1}$, ϕ is proportional to $n_\pm$. With the above numerical values, K_C from Figure 3, and $n_\pm < 7\times10^{28}\text{cm}^{-3}$, $A\Delta t$ should exceed $1.5\times10^9\text{cm}^2\text{sec}$. This condition is well satisfied if the annihilation line is produced over the entire surface of a neutron star, $A \approx 10^{13}\text{cm}^2$, and during the entire impulsive phase of the March 5 event, $\Delta t \approx 0.15$sec (Cline et al. 1980). But the optically thin model would face considerable difficulties

if future measurements should indicate that the line is narrower than 0.2 MeV, or if $A\Delta t$ should turn out, for other reasons, to be smaller than $1.5 \times 10^9 cm^2 sec$ (e.g. if the emitting area covers only a fraction of the polar cap area).

The advantage of producing the annihilation line by grasar action is that a narrow line can form in a hot optically thick region. To illustrate this, we have evaluated the photon intensity perpendicular to a slab of thickness L in which the emissivity and absorption coefficient do not depend on position:

$$I = (j_t/K_t)\{1 - \exp[-K_t L]\} \qquad (42)$$

Using the j_t's and K_t's of Figure 4 ($T_\pm = T_\gamma = 3 \times 10^9 K$, $\mu_\gamma = 0$, $\mu_\pm = 1.1$ MeV), we show in Figure 6 the dependence of I on photon energy E_γ and slab thickness L. As can be seen, grasar action can indeed narrow the line. For example, if $L > 10^{-5} cm$, the width is less than 0.2 MeV. In comparison, the thermal width is ~ 0.8 MeV in an optically thin Maxwell-Boltzmann gas at $3 \times 10^9 K$ (Ramaty and Mészáros 1981, or see $j_{\gamma\gamma}$ in Figure 3).

The peak energy of the annihilation line formed by grasar action is in the range 0.4 to 0.47 MeV, i.e. close to the observed peak energies. Thus, the gravitational redshift of the line due to the compact object which presumably produces the burst should be quite low, $z \lesssim 0.1$. This implies that gamma ray burst sources with observed e^+-e^- emission lines could be objects other than neutron stars, or if they are neutron stars, these stars should have small masses ($M < 0.6 M_\odot$, Börner and Cohen 1973).

Returning to the results of Figure 6, we note that the photon intensities at the centers of the narrow lines entail very large photon occupation numbers. At 0.43 MeV, these numbers, given by $n_\gamma = 4\pi^3 \hbar^3 c^2 E_\gamma^{-2} I(E_\gamma)$, are $n_\gamma = 200$ and 8000 for $L = 10^{-5} cm$ and $2 \times 10^{-5} cm$. The development of such high

photon densities clearly should modify the j's and K's used to calculate the intensity of Figure 6, but we defer the investigation of such a nonlinear system to a subsequent study.

Nevertheless, assuming that an inverted layer with parameters as in Figure 6 did exist in the March 5 burst source region, the line fluence ϕ can be calculated as follows

$$\phi = A\Delta t d^{-2} \int I(E_\gamma) dE_\gamma \tag{43}$$

Using the results of Figure 6 with $L = 10^{-5}$cm and $\phi = 10$ photons cm^{-2}, equation (43) yields $A\Delta t \approx 1.2 \times 10^6$ cm^2sec. By comparing with the minimum $A\Delta t$ deduced above for radiation produced in the last optical depth ($A\Delta t > 1.5 \times 10^9$ cm^2 sec), we see that not only can grasar action produce a narrow line in a much hotter region, but that the observed line intensity and width are consistent with a much smaller source and/or a much shorter line formation time.

V Conclusions

We have carried out a fully relativistic treatment of pair production and annihilation and Compton and inverse Compton scattering in a medium containing photons, positrons, and electrons, with equal e^+ and e^- densities. In the calculation of the emissivities and absorption coefficients we have included the stimulation of transitions caused by the Bose-Einstein nature of the photons and the suppression of transitions due to electron and positron degeneracy. We have shown that for systems in thermodynamic equilibrium the calculations lead to an exact balance between pair production and pair annihilation and between Compton and inverse Compton scatterings. This balance can only be achieved if the above stimulation and suppression effects

are properly taken into account. For systems not in equilibrium, grasar action is possible. We have evaluated, in particular, the absorption coefficient for equal photon and particle temperatures and positive particle chemical potential ($\mu_{\pm}>0$). For this example of population inversion, the total absorption coefficient can become negative due to the much larger probability for stimulated annihilation than for Compton scattering and pair production. This type of grasar action can produce a narrow emission line peaked at an energy of about 0.43 MeV. This energy is lower than the peak of the spontaneous annihilation emissivity, which occurs at energies greater than 0.511 MeV. This is caused by the enhancement of all absorption and stimulated emission effects with decreasing energy by the smaller amount of available phase space which leads to a larger occupation number for the same photon density. In a bath of blackbody photons ($\mu_{\gamma} = 0$) and e^{+}-e^{-} pairs of temperature equal to the photon temperature, the threshold for grasar action is at $\mu_{\pm} = 1$ MeV corresponding to pair densities $\sim 10^{30}cm^{-3}$ for $T = 10^{9}K$. A temperature of $\sim 5x10^{9}K$ is needed to produce this density in equilibrium with blackbody photons.

We have applied our results to gamma ray bursts, in particular to the March 5, 1979 transient from which an emission line at $\sim$ 0.43 MeV was observed (Mazets et. al. 1979). Similar emission lines have been seen from several other bursts as well (Teegarden and Cline 1980, Mazets et.al. 1981). While these lines could be produced in a cool skin layer of the source region (Ramaty et al. 1980, 1981), grasar action has the advantage of being capable of producing a narrow line from a hot and optically thick source and from a source region of relatively small emitting area and short duration of line formation. But if grasar action is responsible for the observed 0.4 to 0.46 MeV emission line seen from gamma ray bursts, then their sources cannot be a

neutron star of mass much larger than about 0.6 M_0. At the surfaces of such neutron stars, the gravitational field would shift the line to an energy lower than observed.

There are several difficulties and shortcomings in our treatment. We have not shown how the inversion ($\mu_t>0$) is produced. It could in principle result from the cooling of the pairs that is faster than their annihilation, or by a rapid external supply of pairs without heating. Cooling by synchrotron emission has already been proposed for gamma ray burst sources (Ramaty et al. 1980, 1981), but for the high densities that we consider here, the required field ($B>10^{12}$gauss) seems to lead to synchrotron self-absorption that could quench the grasar action. We have ignored other effects of a strong magnetic field as well, by limiting our calculations to isotropic distributions and by using plane wave functions instead of Landau functions. This isotropic treatment also does not allow the study of beaming effects which should be present in a gamma ray maser. Finally, we have not made any attempts to study the spatial and temporal development of a system exhibiting grasar action. We expect this development to be highly nonlinear.

We have indicated in the analytic part of the paper that Compton maser action is possible if the photon temperature is higher than the electron temperature and indeed in cases where the photons cannot be characterized by a single temperature. Such maser action could lead to very interesting effects in the 10 to 100 keV region which we have not yet fully explored.

As already indicated, gamma ray burst sources are possible astrophysical sites where grasar action could occur. The most obvious observational test for this would be the observation of a narrow (FWHM << 0.1 MeV) emission line at ~ 0.43 MeV.

References

Aharonian, F. A., Atoyan, A. M., and Sunyaev, R. A. 1980, Yerevan Physics Institute Preprint EFI 432(39)-80.

Barat, S., Chambon, G., Hurley, K., Niel, M., Vedrenne, G., Estulin, I. V., Kurt, V. G. and Zenchenko, V. M. 1979, Astron. and Astrophys. 79, L24.

Bekefi, G. 1966, Radiation Processes in Plasmas (Wiley: New York).

Borner, G. and Cohen, J. M. 1973, Ap. J. 185, 959.

Cavallo, G. and Rees, M. J. 1978, Monthly Notices Roy. Astron. Soc. 183, 359.

Cline, T. L. 1981, Proc. 10th Texas Symposium on Relativistic Astrophys. (N.Y. Acad. of Sci., in press).

Cline, T. L. et al. 1980, Ap. J. 237, L1.

Evans, W. D. et al. 1980, Ap. J. 237, L7.

Gould, R. J. and Schreder, G. P. 1967, Phys. Rev. 155, 1404.

Jauch, J. M. and Rorlich, F. 1955, The Theory of Photons and Electrons (Addison-Wesley: Reading, Mass).

Landau, L. D. and Lifshitz, E. M. 1958 Statistical Physics (Pergamon Press: London).

Mazets, E. P., Golenetskii, S. V., Aptekar, R. L., Guryan, Yu. A. and Ilyinskii, V. N. 1981, Nature 290, 378.

Mazets, E. P., Golenetskii, S. V., Ilyinskii, V. N., Aptekar, R. L. and Guryan, Yu. A. 1979, Nature 282, 587.

Ramaty, R., Bonazzola, S., Cline, T. L., Kazanas, D., Mészáros, P. and Lingenfelter, R. E. 1980, Nature 287, 122.

Ramaty, R., Lingenfelter, R. E. and Bussard, R. W. 1981, Astrophys. Space Sci. 75, 193.

Ramaty, R. and Mészáros, P. 1981, Ap. J. 250 (in press).

Schmidt, W. K. H. 1978, Nature, 271, 525.

Teegarden, B. J. and Cline, T. L. 1980, Ap. J. Lett. 236, L67.

Varma, C. M. 1977, Nature 267, 686.

Zdziarski, A. A. 1981, Acta Astronomica (in press).

Figure Captions

1. Density of photons and pairs vs. temperature. The line labelled γ represents blackbody photons. The curves labelled by values of the pair chemical potential $\mu_{\pm}$ represent pairs in a Fermi-Dirac distribution.
2. Emissivities and absorption coefficients vs. photon energy in a system in thermodynamic equilibrium at 3×10^9K. The Compton emissivity (not shown) is the difference between the total emissivity j_t and the annihilation emissivity $j_{\gamma\gamma}$. The Compton absorption coefficient (not shown) is the difference between the total absorption coefficient K_t and the pair production absorption coefficient $K_{\gamma\gamma}$. The photon and pair densities in these conditions are 5.5×10^{29}cm^{-3} and 2.4×10^{29}cm^{-3} respectively.
3. Emissivities and absorption coefficients vs. photon energy in a system at 3×10^9K having equilibrium between pair annihilation and pair production by non-blackbody photons with chemical potential -2.0 MeV. The curves have the same significance as in Figure 2. The photon and pair densities in these conditions are 2.0×10^{26}cm^{-3} and 1.0×10^{26}cm^{-3} respectively.
4. Emissivities and absorption coefficients vs. photon energy in a system at 3×10^9K with blackbody photons and an inverted pair population described by pair chemical potential 1.1 MeV. The curves have the same significance as in Figure 2 except that the Compton absorption coefficient K_C is shown explicitly. Negative values of total and pair production absorption coefficients are represented by dashed curves. The photon and pair densities in these conditions are 5.5×10^{29} cm^{-3} and 7.3×10^{30}cm^{-3} respectively.
5. Emissivities and absorption coefficients vs. photon energy in a system at zero temperature with fully degenerate pairs described by chemical

potential 0.85 MeV. The curves have the same significance as in Figure 4. The photon and pair densities in these conditions are zero and $1.4 \times 10^{30} cm^{-3}$ respectively.

6. The development of the intensity of the annihilation line with increasing thickness of source. The system is the same as that for Figure 4. The labels on successive maxima indicate the thickness involved, and the peak energy and FWHM of the line.

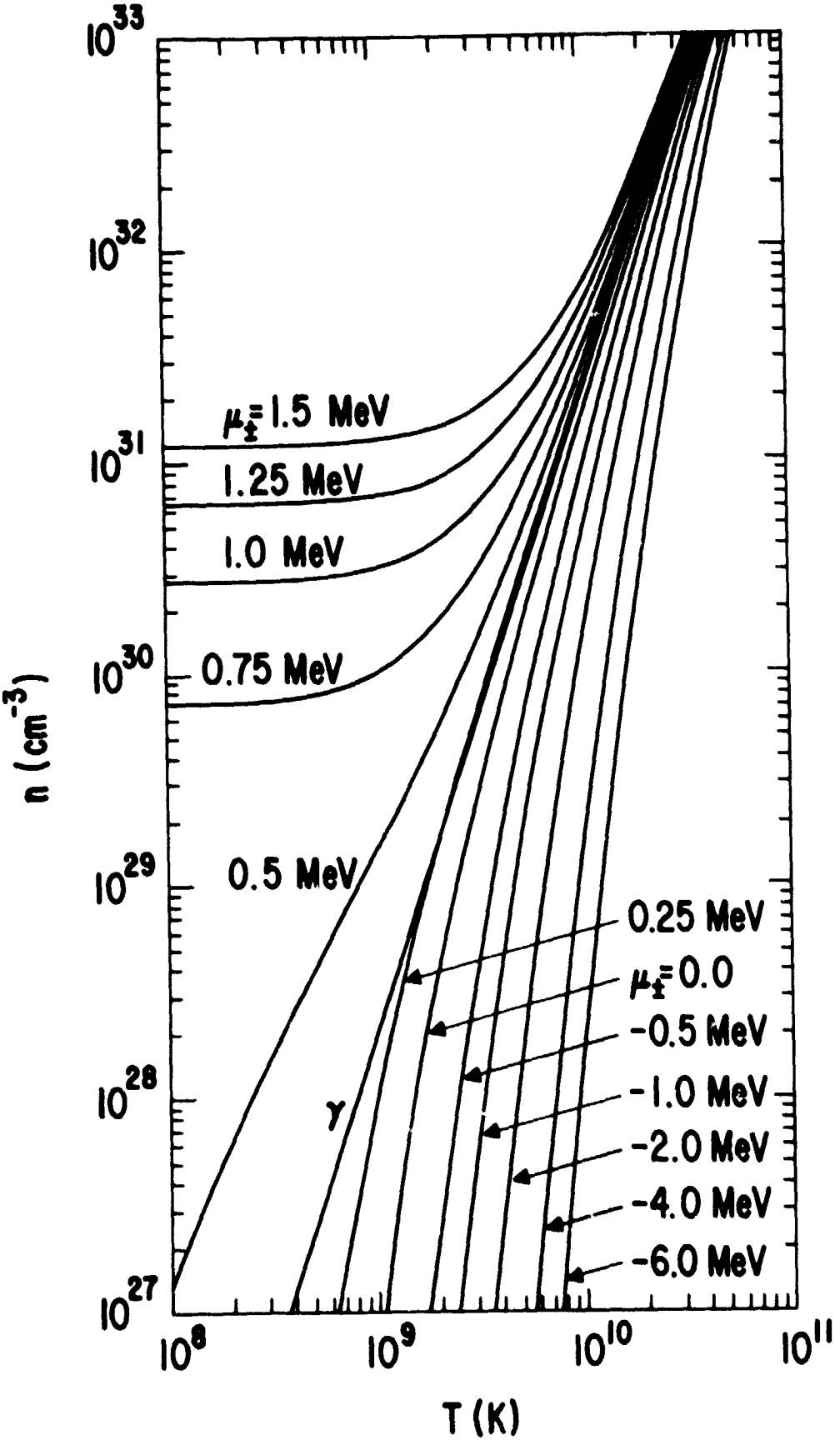
10^{33}
10^{32}
10^{31}
10^{30}
10^{29}
10^{28}
10^{27}
n (cm^{-3})
μ_Σ=1.5 MeV
1.25 MeV
1.0 MeV
0.75 MeV
0.5 MeV
γ
0.25 MeV
μ_Σ=0.0
-0.5 MeV
-1.0 MeV
-2.0 MeV
-4.0 MeV
-6.0 MeV
10^8
10^9
10^{10}
10^{11}
T (K)

Figure 1

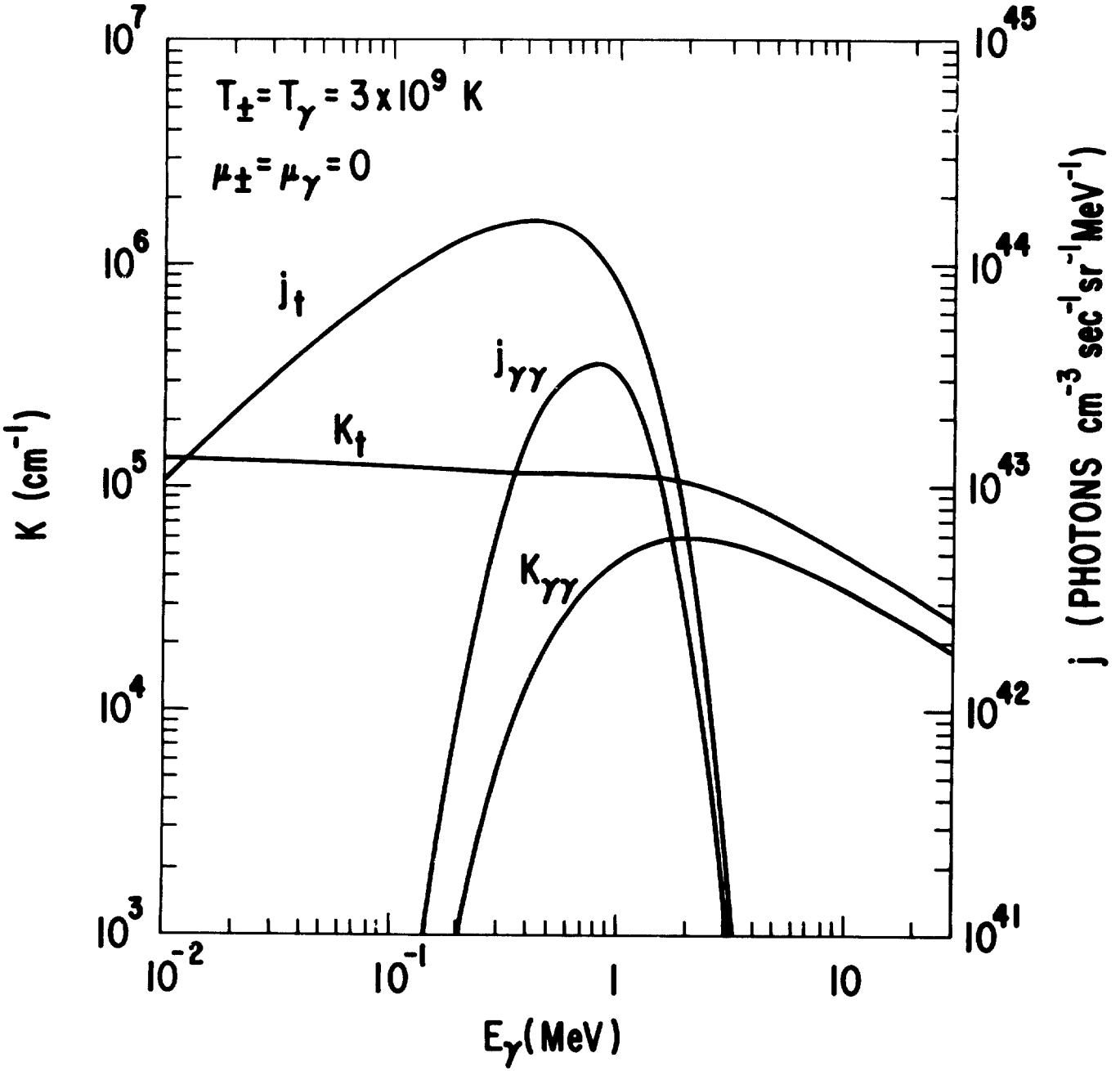
$T_\pm = T_\gamma = 3 \times 10^9$ K
$\mu_\pm = \mu_\gamma = 0$
j_t
$j_{\gamma\gamma}$
K_t
$K_{\gamma\gamma}$
K (cm^{-1})
j (PHOTONS cm^{-3} sec^{-1} sr^{-1} MeV^{-1})
E_γ(MeV)
10^7
10^6
10^5
10^4
10^3
10^{45}
10^{44}
10^{43}
10^{42}
10^{41}
10^{-2}
10^{-1}
1
10

Figure 2

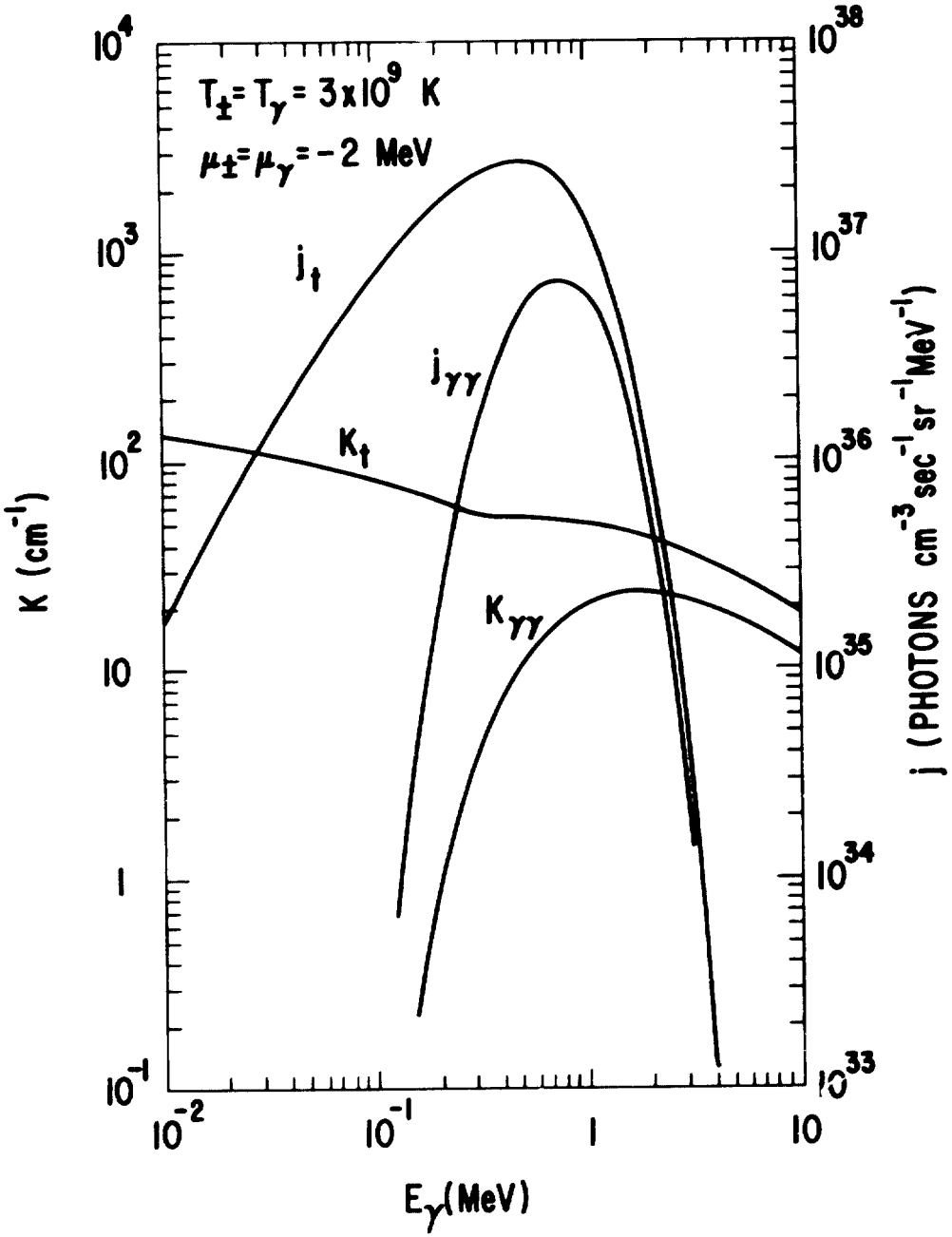
$T_\pm = T_\gamma = 3 \times 10^9$ K
$\mu_\pm = \mu_\gamma = -2$ MeV
j_t
$j_{\gamma\gamma}$
K_t
$K_{\gamma\gamma}$
K (cm^{-1})
j (PHOTONS $cm^{-3} sec^{-1} sr^{-1} MeV^{-1}$)
E_γ(MeV)
10^4
10^3
10^2
10
1
10^{-1}
10^{38}
10^{37}
10^{36}
10^{35}
10^{34}
10^{33}
10^{-2}
10^{-1}
1
10

j (PHOTONS cm^{-3}sec^{-1}sr^{-1}MeV^{-1})
10^{47}
10^{46}
10^{45}
10^{44}
10^{43}
10^{42}
$K_{\gamma\gamma}$
K_C
K_t
$j_{\gamma\gamma}$
j_t
— K > 0
--- K < 0
$T_\pm = T_\gamma = 3 \times 10^9$ K
$\mu_\pm = 1.1$ MeV
10^{-2}
10^{-1}
10^{0}
10^{1}
E_γ (MeV)
10^{9}
10^{8}
10^{7}
10^{6}
10^{5}
10^{4}
K (cm^{-1})

Figure 4

j (PHOTONS cm^{-3} sec^{-1} sr^{-1} MeV^{-1})
10^{46}
10^{45}
10^{44}
10^{43}
10^{42}
10^{41}
10
$j_{\gamma\gamma} = j_t$
K_C
$K_{\gamma\gamma}$
K_t
K > 0
K < 0
$T_\pm = T_\gamma = 0$
$\mu_\pm = 0.85$ MeV
10^{-2}
10^{-1}
1
E_γ(MeV)
10^6
10^5
10^4
10^3
K (cm^{-1})

Figure 5

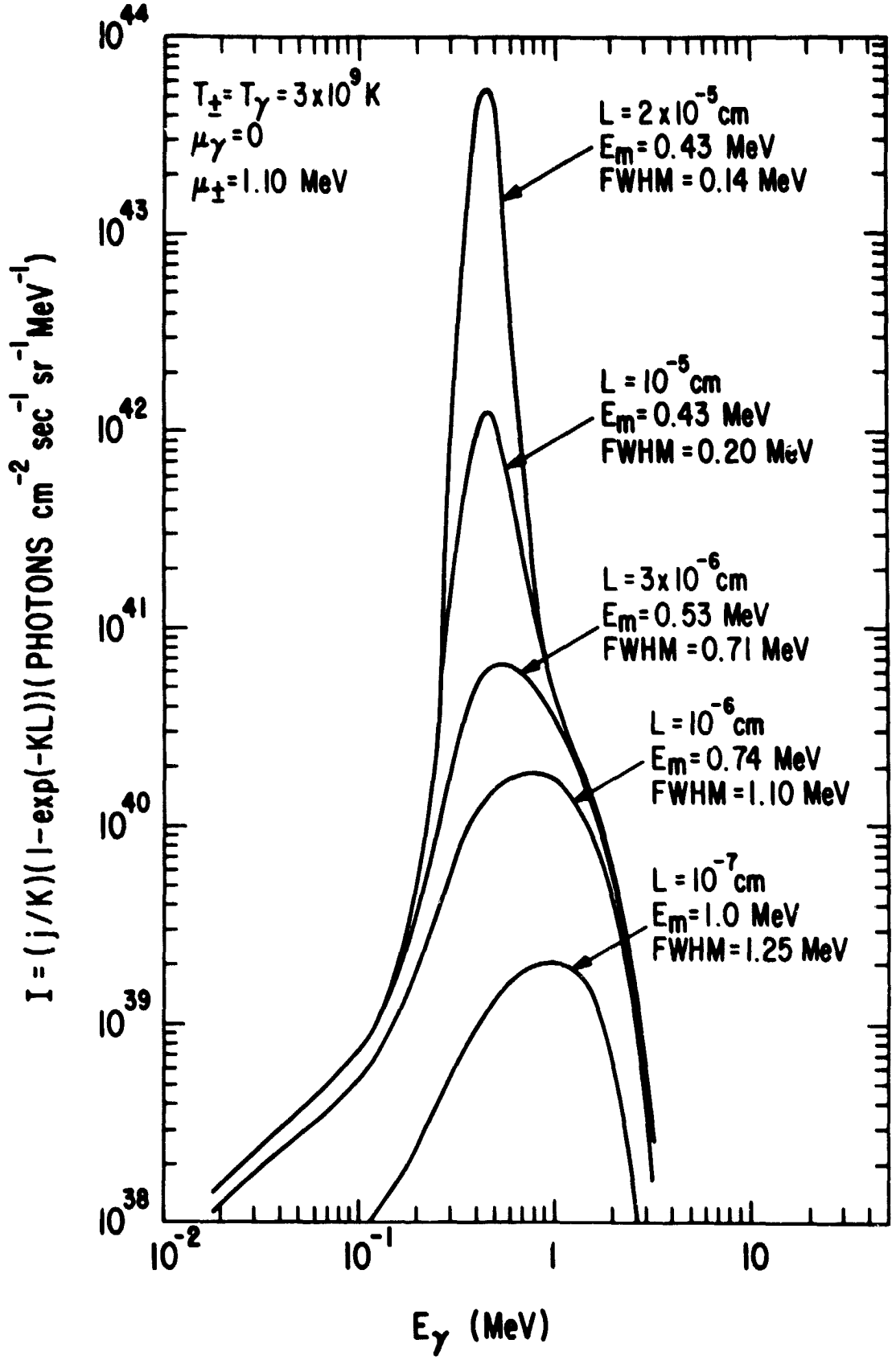
$T_{\pm} = T_{\gamma} = 3 \times 10^{9}$ K
$\mu_{\gamma} = 0$
$\mu_{\pm} = 1.10$ MeV
L = 2×10^{-5} cm
E_m = 0.43 MeV
FWHM = 0.14 MeV
L = 10^{-5} cm
E_m = 0.43 MeV
FWHM = 0.20 MeV
L = 3×10^{-6} cm
E_m = 0.53 MeV
FWHM = 0.71 MeV
L = 10^{-6} cm
E_m = 0.74 MeV
FWHM = 1.10 MeV
L = 10^{-7} cm
E_m = 1.0 MeV
FWHM = 1.25 MeV
$I = (j/K)(1-\exp(-KL))$ (PHOTONS cm^{-2} sec^{-1} sr^{-1} MeV^{-1})
E_{γ} (MeV)

Figure 6